

Electronic Supplementary Information:

**O₂ Adsorption dependent Photoluminescence Emission from
Metal Oxide Nanoparticles**

Amir R. Gheisi¹, Chris Neygandhi¹, Andreas K. Sternig¹,

¹ Institute of Particle Technology, Friedrich-Alexander University Erlangen-Nürnberg,
Erlangen, Germany

Esther Carrasco², Hubertus Marbach²

² Lehrstuhl für Physikalische Chemie II, Friedrich-Alexander University Erlangen-
Nürnberg, Erlangen, Germany

Daniel Thomele³, Oliver Diwald³

³ Department of Materials Science & Physics, Paris-Lodron University of Salzburg,
Salzburg, Austria

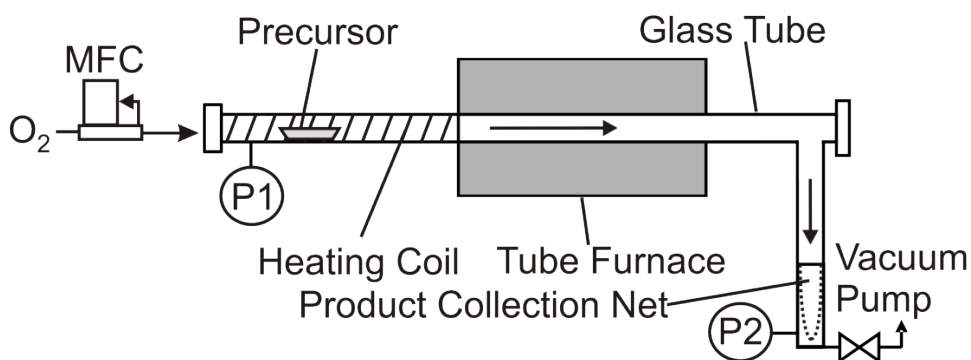


Figure S1: Schematic of the reactor used for production of ZnO nanoparticles.

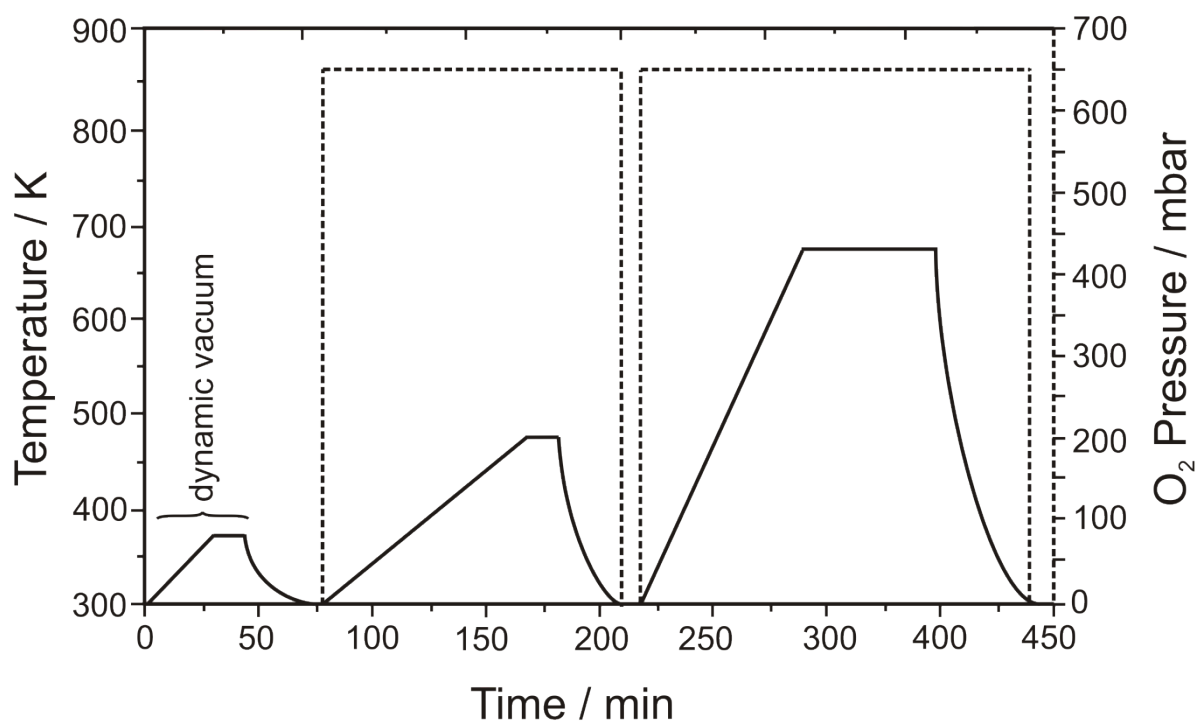


Figure S2: Temperature profile (solid line, left ordinate scale) and applied oxygen pressure (dashed line, right ordinate scale) during annealing treatment.

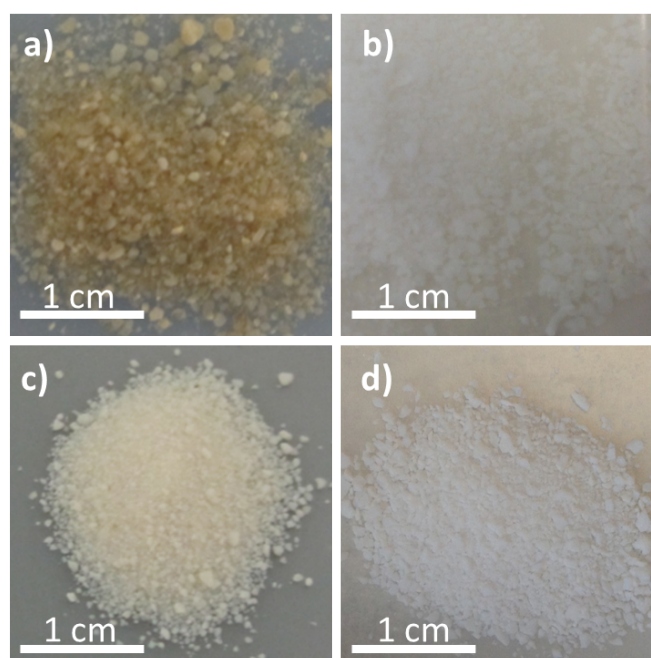


Figure S3: Photos taken from powder samples after synthesis: **a)** ZnO, **b)** MgO; and after annealing in oxygen ($T = 673$ K, $p = 650$ mbar O_2): **c)** ZnO, **d)** MgO.

Analysis of the XRD reflexes widths.

Pseudo-Voigt functions were used to determine the full-width at half maximum (FWHM) of the main reflexes and the average crystallite sizes were calculated with the Scherrer equation¹:

$$D = K\lambda / [W \cos(\theta)]$$

K is a constant which depends on the particle morphology and varies from 0.89 to 1.39 rad. Here K = 1 was used, which corresponds to an average volume of the apparent size D independently of a particular morphology.² λ is the wavelength of CuK α radiation (in nm), W is the full width at half-maximum (FWHM in radian), and θ is the diffraction angle (deg.).

XRD and particle size of MgO nanoparticles

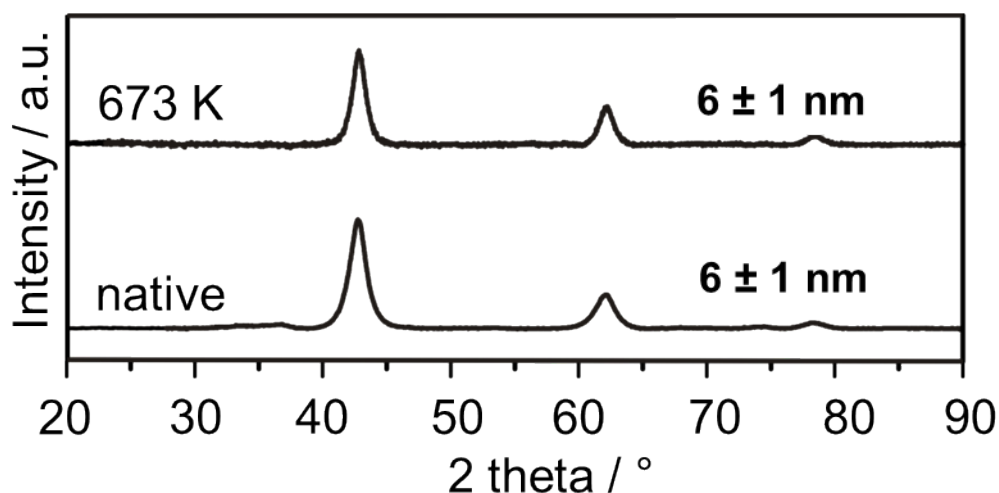


Figure S4: Powder XRD data of MgO nanoparticles after synthesis and after annealing to 673 K.

FT-IR spectroscopy

The infrared spectra of the samples were measured by the attenuation total reflection (ATR) technique using a Varian FTS-3100 spectrometer. The FT-IR experiments were performed under ambient conditions. A small amount of sample powder was

casted on the ATR crystal. A total of 64 scans were accumulated for each spectrum to obtain a reasonable signal to noise ratio with a spectral resolution of 4 cm^{-1} .

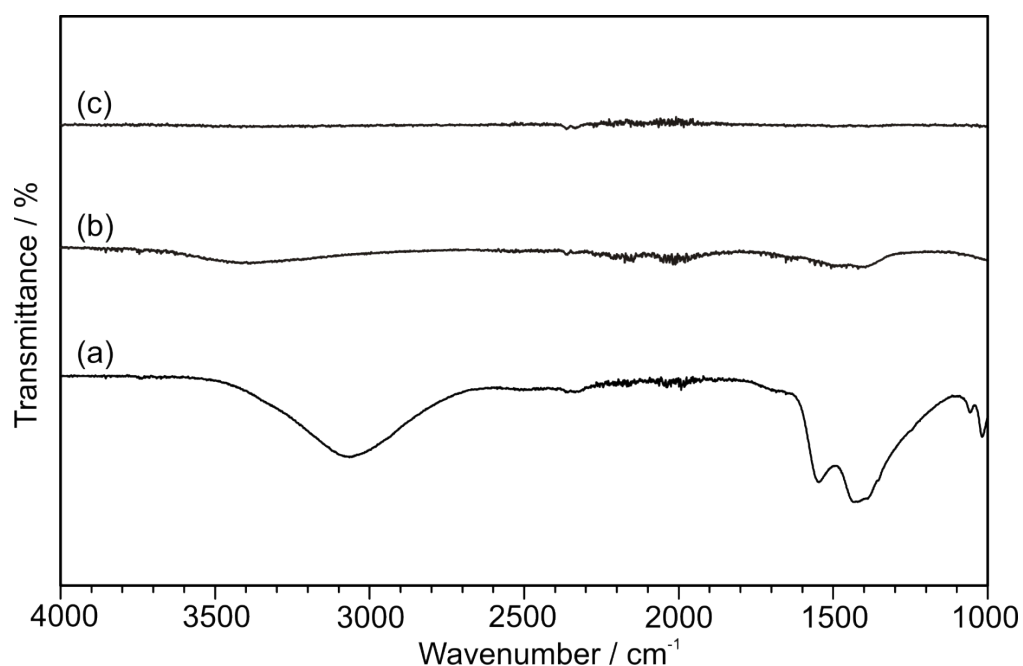


Figure S5: Infrared spectra of a) Zinc acetate dihydrate (precursor used to synthesize ZnO); b) ZnO nanoparticles after synthesis; c) ZnO nanoparticles after subsequent annealing in oxygen ($T = 673\text{ K}$, $p = 650\text{ mbar O}_2$). All the spectra were recorded in air and at room temperature.

ATR-Infrared spectroscopy measurements were performed to investigate the potential presence of synthesis related organic remnants or surface adsorbed species which originate from oxidation of the precursor during annealing. An IR spectrum of the precursor clearly shows absorption peaks between 1110 cm^{-1} and 1730 cm^{-1} that are attributed to the fingerprint of the stretching modes of the acetate groups (COOH).³ In addition to the dihydrate of the precursor salt, also water from ambient adsorbs on the sample powder and results in a broad absorption feature between 2600 cm^{-1} and 3550 cm^{-1} . It is noticeable that for the sample after synthesis all the absorption band intensities decrease upon decomposition and oxidation reaction of the precursor at 1073 K which corresponds to the temperature of the flow

reactor during ZnO synthesis. All features are completely removed from ZnO sample in the course of annealing. Since the ATR-IR studies were carried out in the ambient but shortly after synthesis and annealing treatment, the above results indicate that the density of the acetate and hydroxyl groups remarkably decreases by synthesis and post-treatment conditions applied.

Surface composition analysis by Auger electron spectroscopy

Before quantification and consistent with reference 4, all the spectra in this study have been divided by the kinetic energy E . Since the intensity/ energy response function (IERF) for AES instruments operated in the constant retardation ratio is proportional to $E \cdot \Delta(E)$, i.e. proportional to the product of the kinetic energy by the detector efficiency $\Delta(E)$ [see for example 4], an additional correction to E^{-1} is necessary. This has been checked by using it with AES of a MgO sample previously annealed at around 1073 K in the UHV system (to avoid the presence of contaminations) and following the evaluation procedure with this stoichiometric compound. A minor correction over the factor E^{-1} was necessary in the O region of $E^{-0.985}$ and none in the Mg, validating essentially the procedure. These small corrections were included in the evaluations for ZnO in Table S1 though.

Table S1 compares the atomic O/ Zn ratios for the ZnO nanoparticle characterized in this study with results obtained on different atomically clean ZnO single crystals faces reported in reference.^{4,5}

TABLE S1	
Sample	Atomic ratio O/Zn
Single crystal ZnO	
(from Ref. 5)	
Prism Face	1,15
Zinc Face	1,05
Oxygen Face	1,25
Annealed ZnO	
Derivative analysis	1,29 ± 0,06
Area analysis	1,19 ± 0,14
As-synthesized ZnO	
Derivative analysis	1,41 ± 0,04
Area analysis	1,50 ± 0,12

Photoluminescence spectroscopy

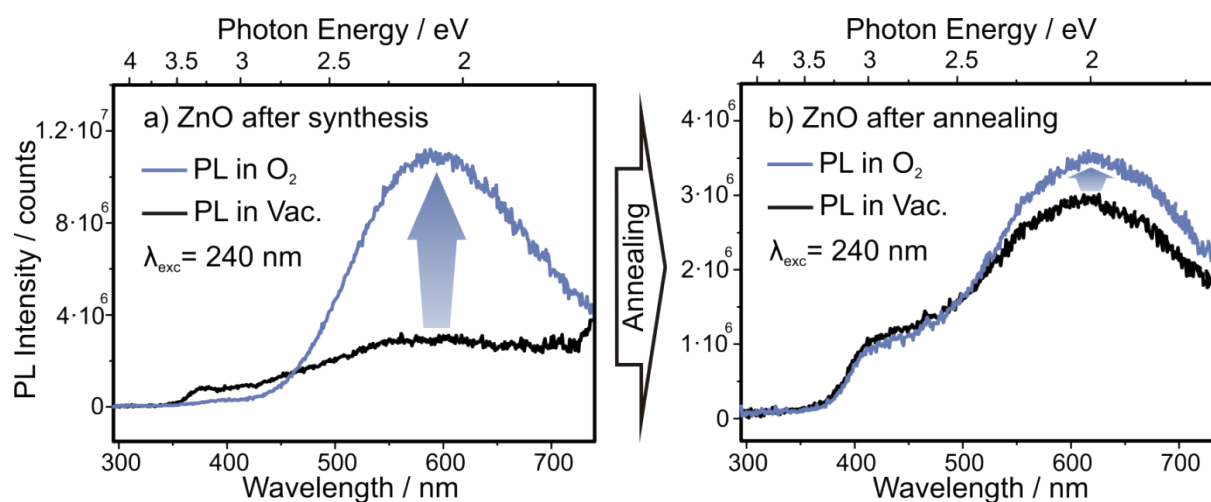


Figure S6: Photoluminescence (PL) spectra of a) ZnO after synthesis; b) ZnO after annealing in oxygen ($T = 673 \text{ K}$, $p = 650 \text{ mbar O}_2$); Samples are excited at 240 nm and for each of them PL spectra are recorded at $T = 298 \text{ K}$ and in two environments: 1) 10 mbar O_2 ; 2) $p < 10^{-5} \text{ mbar}$.

Figure S6 shows the PL emission spectra of ZnO sample obtained upon excitation with $h\nu_{Exc} = 5.2 \text{ eV}$ ($\lambda_{Exc} = 240 \text{ nm}$). Figures S6a and S6b indicate for ZnO that

excitation at $h\nu_{\text{Exc}} = 5.2 \text{ eV}$ produces qualitatively the same emission feature as excitation at $h\nu_{\text{Exc}} = 4.6 \text{ eV}$ ($\lambda_{\text{Exc}} = 270 \text{ nm}$).

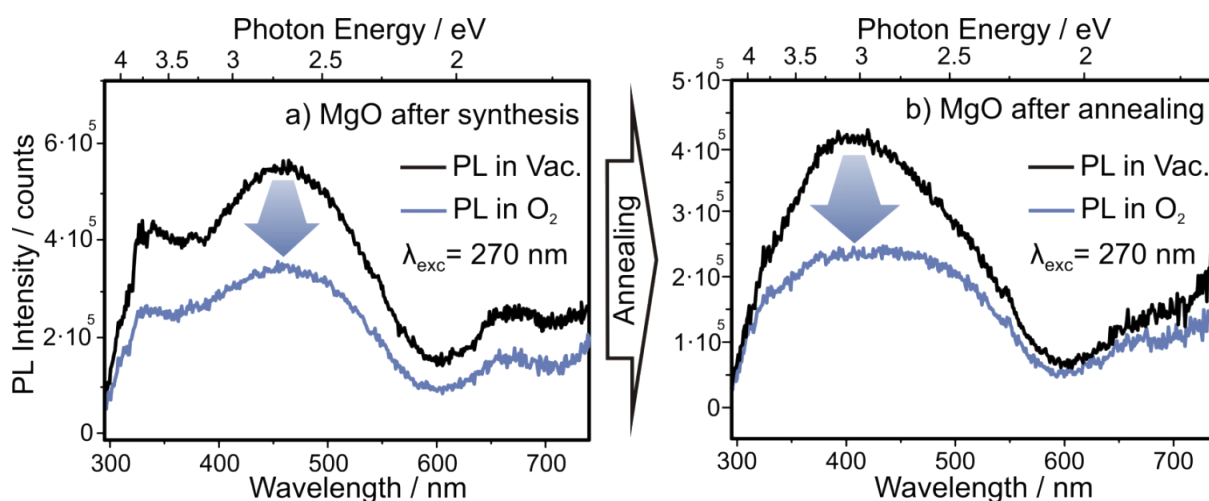


Figure S7: Photoluminescence (PL) spectra of **a)** MgO nanoparticles after synthesis; **b)** MgO nanoparticles after annealing in oxygen ($T = 673 \text{ K}$, $p = 650 \text{ mbar O}_2$). Samples are excited at $h\nu_{\text{Exc}} = 4.6 \text{ eV}$ and corresponding PL spectra are recorded at $T = 298 \text{ K}$ either in 1) 10 mbar O_2 or in 2) $p < 10^{-5} \text{ mbar}$.

Figure S7a reveals the emission spectrum for well dispersed MgO nanoparticles just after synthesis. Whereas fully dehydroxylated MgO nanocubes excitation at $h\nu = 4.6 \text{ eV}$ ($\lambda_{\text{exc}} = 270 \text{ nm}$) leads to corner excitation and produces one PL emission band centered at $h\nu = 3.3 \text{ eV}$ ($\lambda_{\text{Em}} = 380 \text{ nm}$), here one excitation process contributes to the photoluminescence emission. Subsequent annealing treatment ($T = 673 \text{ K}$ and $p = 650 \text{ mbar O}_2$) on MgO changes the shape of spectra due to partial dehydroxylation of the sample surface and a band centered at $\lambda_{\text{Em}} = 400 \text{ nm}$ is present (Figure S7b). Figure S7a and S7b both prove that unlike ZnO, PL emission of MgO is quenched in O_2 atmosphere.

References

- 1 C. Weidenthaler, *Nanoscale*, 2011, **3**, 792–810.
- 2 A. Weibel, R. Bouchet, F. Boulc' and P. Knauth, *Chem. Mater.*, 2005, 17, 2378–2385.
- 3 Y. Xia, Y. Xiong, B. Lim and S. E. Skrabalak, *Angewandte Chemie - International Edition*, 2009, **48**, 60–103.
- 3 S. Mroczkowski and D. Lichtmann, *J. Vac. Sci. Technol. A*, 1985, **3**, 1860.
- 4 D. Briggs and J. T. Grant, *Surface analysis by Auger and x-ray photoelectron spectroscopy*, IM Publications, Chichester, 2003.
- 5 S. Z. Weisz, O. Resto, G. Yaron, A. Many and Y. Goldstein, *J. Vac. Sci. Technol. A*, 1987, **5**, 302